# Electronic Supplementary Information

## Urea-Based Polyphenol Receptor Demonstrate Colorimetric and Fluorometric Detection of Cyanide in Real-life Applications

Sanjana Das and Gopal Das*

Department of Chemistry, Indian Institute of Technology Guwahati, Assam, 781039, India

E-mail: gdas@iitg.ac.in

**S1. Materials and Instrumental Techniques.** All the reagents, solvents, and chemicals for synthesis were purchased from commercially available sources (Sigma-Aldrich Chemical Co.) and used without further purification. All the used solvent was analytical reagent (AR) grade. PerkinElmer Lamda25 UV/Visible spectrophotometer was used to measure absorption spectra using 1 cm path-length quartz cuvettes. For fluorescence measurements, we employed a Horiba Fluoromax-4 spectrofluorometer with a slit width of 5 nm operating at 298 K, using 1 cm path-length quartz cuvettes. High-resolution mass spectra were recorded using an Agilent LC_QTOF_HRMS Premier mass spectrometer using the ESI mode. A Bruker Advance 600 MHz instrument was used to record $^{1}H$ and $^{13}C$ Nuclear Magnetic Resonance (NMR) spectra using DMSO-$d_6$ as a solvent, with chemical shifts recorded in parts per million (ppm) scale. We employed the following abbreviations to describe spin multiplicities in the $^{1}H$ NMR spectra: s=singlet; d=doublet; t=triplet; q=quartet; and m=multiplet. We recorded (FTIR) measurements of the samples using a Bruker VERTEX 70v FTIR spectrometer. The pH measurement was carried out with an Orion 3 Star pH Benchtop meter.

**S2. UV−Vis and Fluorescence-Spectroscopy Studies.** The stock solutions of all the anions (using n-Tetrabutylammonium salts of the corresponding anions) were prepared in DMSO at a concentration of 50 mM. Additionally, stock solutions of NPH (5mM) and NPN (5mM) were also prepared in DMSO and then diluted to a concentration of 5Mm in MilliQ water for various spectroscopy studies. This was done by adding just 3.0 μL of NPH or NPN stock solution in MilliQ water to a final volume of 3 mL. In the fluorescence/UV-Vis sensing experiment, we prepared the test samples by mixing the right amounts of the stock solutions of the anions into 3 mL of aqueous probe solution. The aqueous probe solution contained 5 μM of probe and 0.2% DMSO. For the fluorescence titration experiments, we made a 50 mM stock solution of TBACN (n-Tetrabutylammonium cyanide) in DMSO and then added it gradually into a 3 mL aqueous probe solution using a micropipette in a quartz optical cell with 1.0 cm path lengths. All the experiments were done in pH=6.

**S3. Limit of Detection (LOD).** Using UV-Vis titration and fluorescence titration experiments as a basis, we calculated the detection limit (LOD). The absorbance spectrum as well as fluorescence emission spectrum of NPH was measured 10 times, and the standard deviation (σ) of blank measurement was also attained from the experiment. We plotted the absorbance

and fluorescence emission values to the concentration of $CN^-$ (obtained from the UV-Vis and fluorescence titration experiment). The slope of the fitted straight line (k) was calculated from the plot and finally detection limit was calculated using the following equation:

$$LOD = 3\sigma/K \quad \text{---------- (1)}$$

Where σ is the standard deviation of blank measurement, and K is the slope between the absorbance/fluorescence emission intensity versus concentration of $CN^-$.

**S4. Morphology Analyses**

The morphology of NPH, NPN, and NPH + $CN^-$ complexes was examined using Field Emission Scanning Electron Microscopy (FESEM) techniques. A Carl Zeiss Gemini 300 FESEM was used to photograph the morphologies of each sample independently. Before imaging, the samples were prepared by drop-casting 2 μL of the desired solution combination on an Al-foil-wrapped coverslip, followed by coating with Au and drying under vacuum.

**S5. Dynamic Light Scattering Studies.** Dynamic light scattering (DLS) is a technique used to measure the particle size distribution of samples in solution by analyzing the intensity of scattered light. The particle size of both probes, NPH and NPN, was determined through dynamic light scattering (DLS) experiments conducted on a Malvern Zetasizer Nano ZS instrument. This instrument was equipped with a 4.0 mW HeNe laser that operated at a wavelength of 633 nm. All the measurements were done at room temperature (25°C).

**S6. Quantum Yield Calculation**

The quantum yield (Φ) was determined by comparing the integrated photoluminescence intensities and absorbance values of NPH with quinine sulfate (QS) as the reference as shown in Tabe S2. Quinine sulfate (with a known Φ value of 0.54 from the literature) was dissolved in 0.1 M $H_2SO_4$, which has a refractive index (η) of 1.33. The receptors were dissolved in distilled water, also with a refractive index of 1.33. In this context, Φ represents the quantum yield, I represent the measured integrated emission intensity, and η is the refractive index. The absorbance at the excitation wavelength of 380 nm of the quinine sulfate and receptors is denoted by $A_R$ and A, respectively. The subscript R refers to the reference fluorophore of known quantum yield.

$$\Phi = \Phi_R \times \frac{I}{I_R} \times \frac{A_R}{A} \times \frac{\eta^2}{\eta_R^2} \quad \text{---------- (2)}$$

## S7. Time-resolved fluorescence spectroscopy

Fluorescence lifetimes were evaluated utilizing the time-correlated single-photon counting (TCSPC) set-up from Horiba instruments. As a source, a laser diode with an excitation wavelength of 380 nm was employed with an instrument response function IRF. The fluorescence decays were made to fit through exponential decay. Both NPH and NPH + $CN^-$ were fitted into double exponential decay.

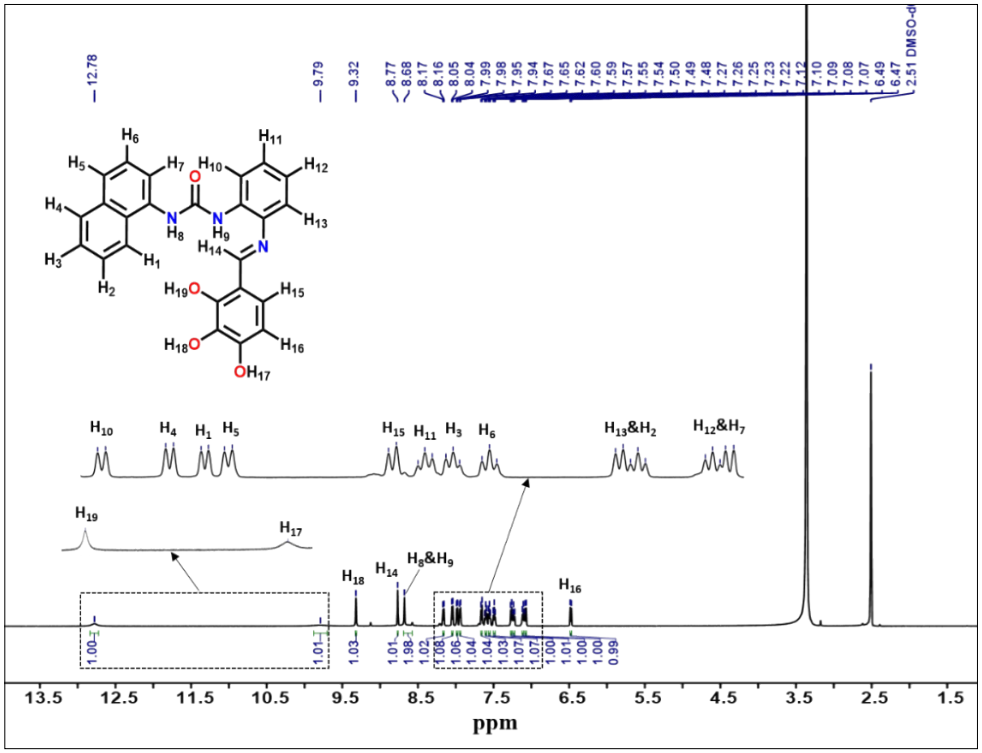


**Fig. S1** $^1$H NMR spectrum of NPH in DMSO-$d_6$.

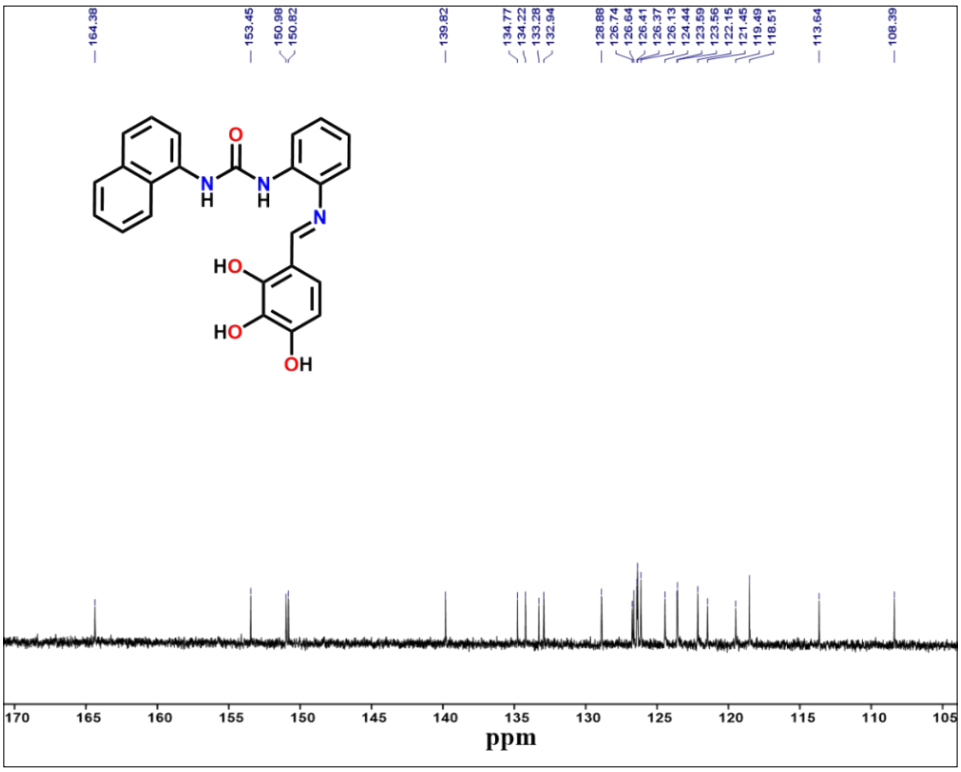


**Fig. S2** $^{13}$C NMR spectrum of NPH in DMSO-$d_6$.

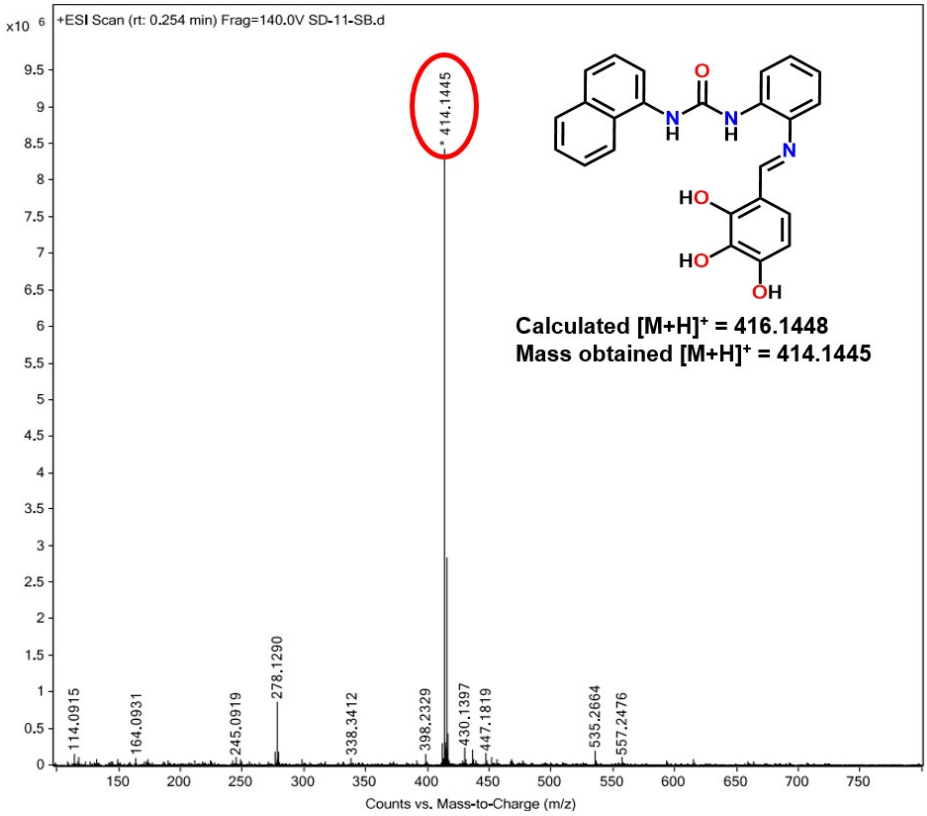


**Fig. S3** HRMS of NPH.

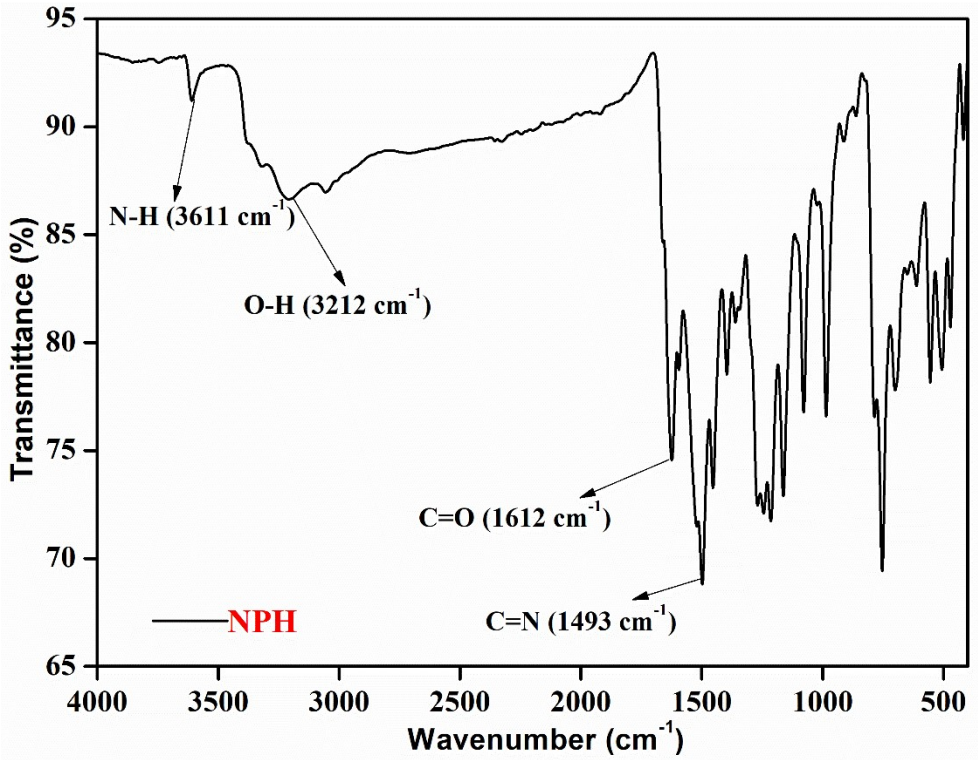


**Fig. S4** IR Spectrum of NPH.

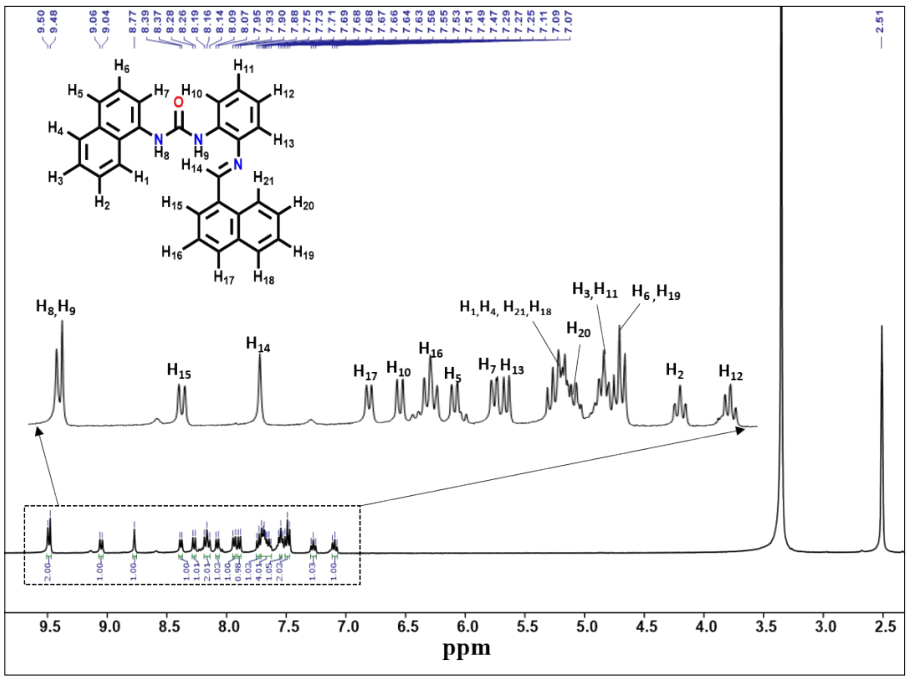


**Fig. S5** $^{1}$H NMR spectrum of NPN in DMSO-$d_6$.

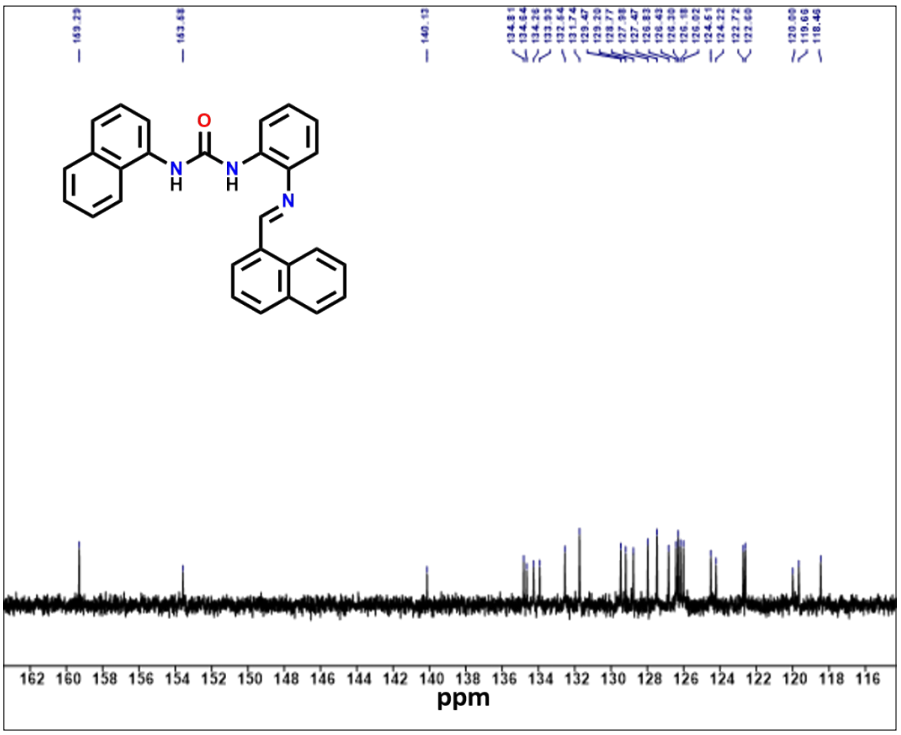


**Fig. S6** $^{13}$C NMR spectrum of NPN in DMSO-$d_6$.

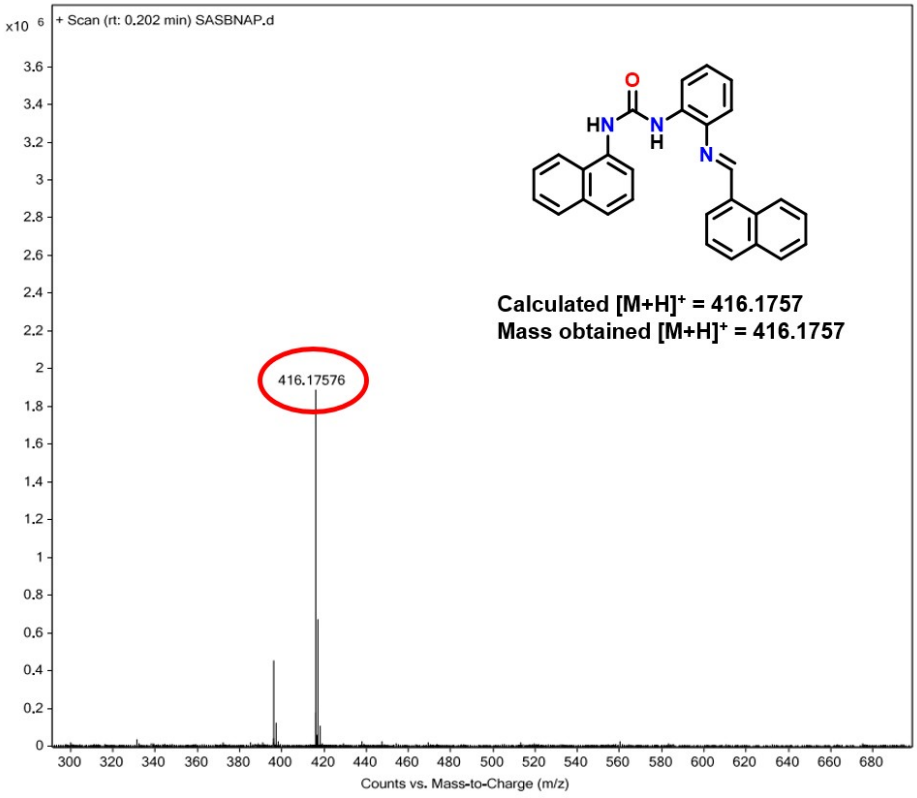


**Fig. S7** HRMS of NPN.

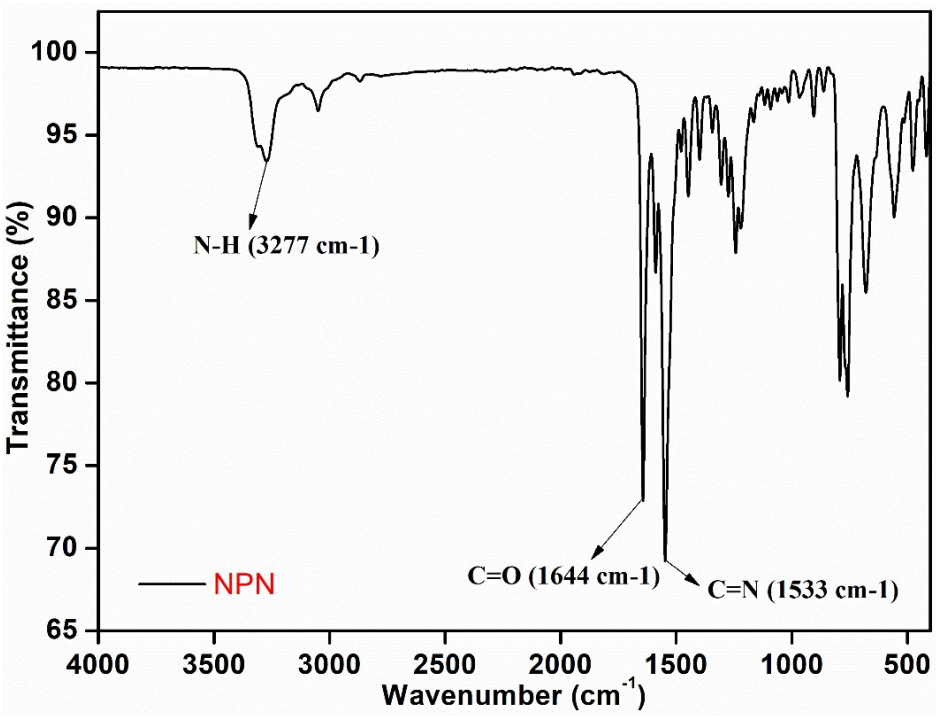


**Fig. S8** FTIR spectra of NPN.

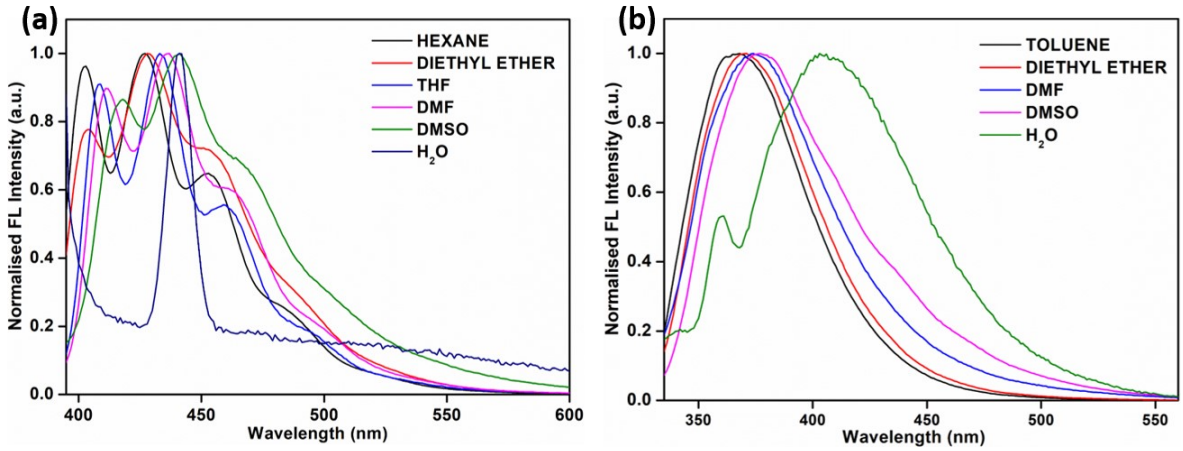


**Fig. S9** Normalised emission spectra of (a) NPH, and (b) NPN in different solvents.

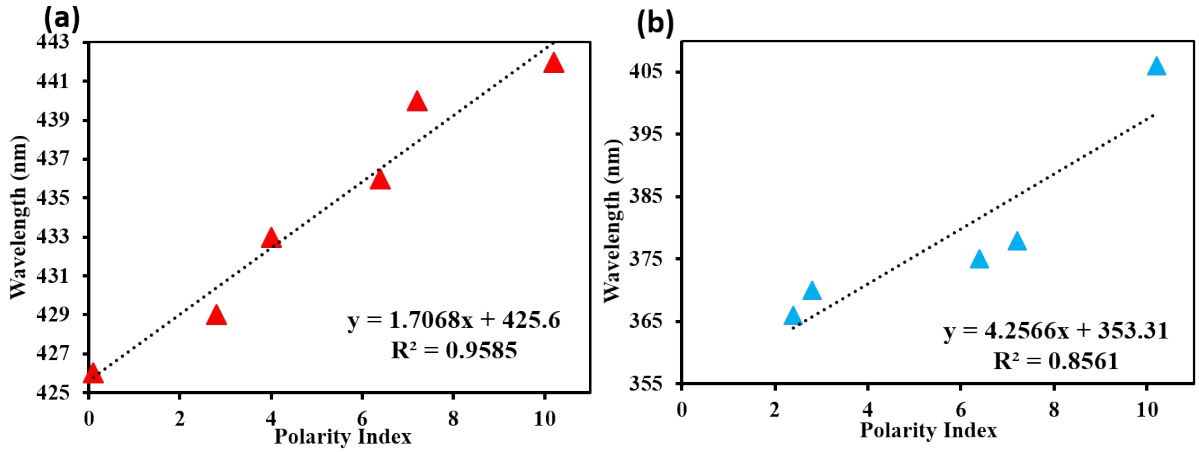


**Fig. S10** Correlation of emission wavelength vs. polarity index of (a) NPH, and (b) NPN in different solvent media.

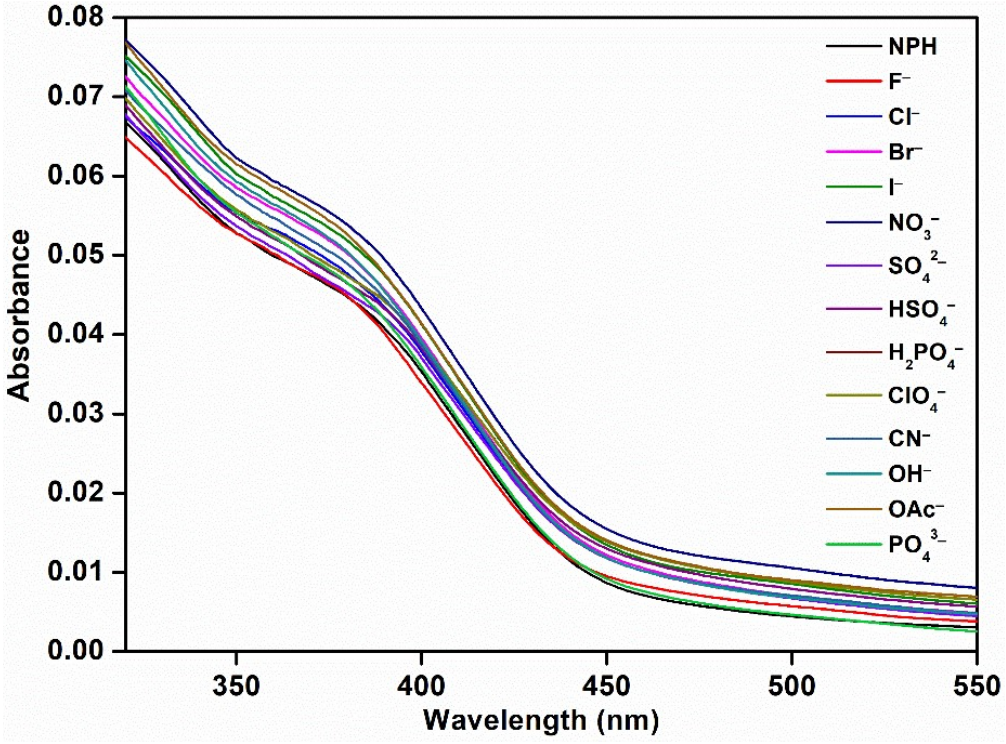


**Fig. S11** UV-Vis Spectrum of NPN with various anions.

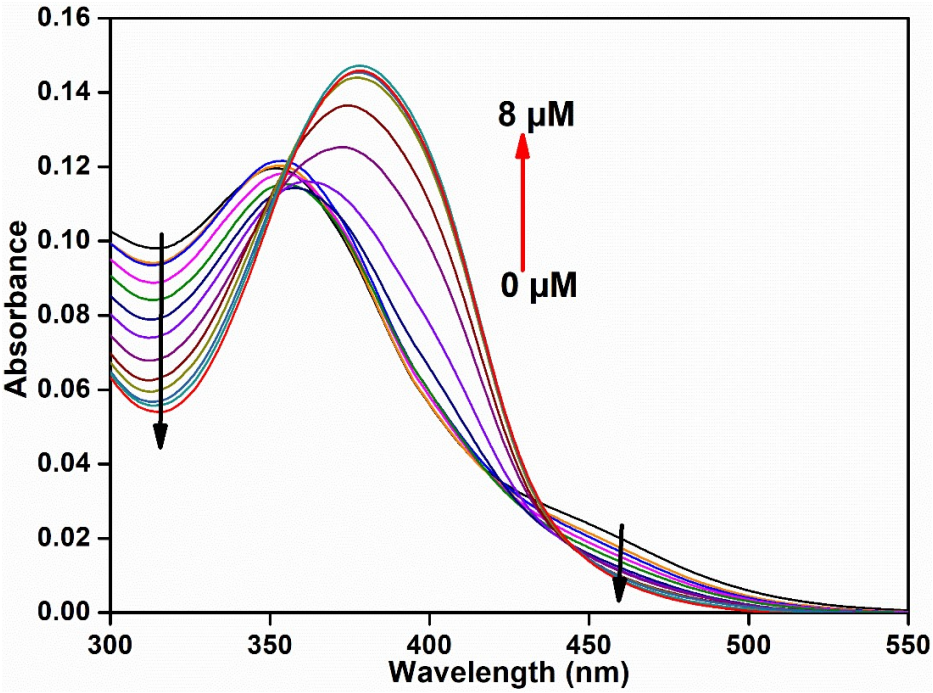


**Fig. S12** (a) UV-Vis titration of NPH with $CN^-$ (0-8µM).

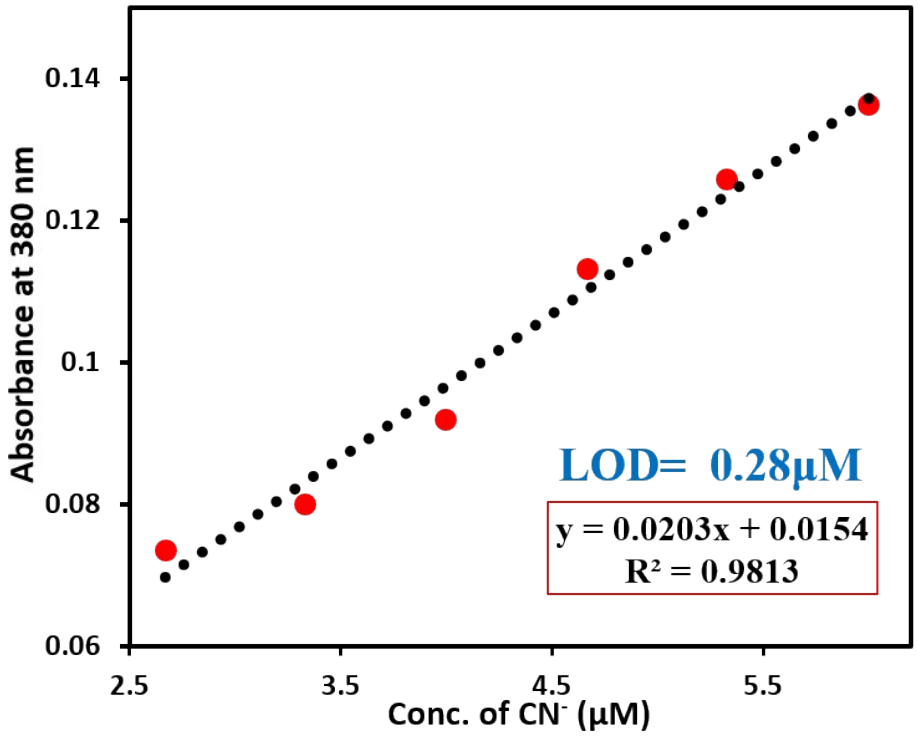


**Fig. S13** Absorbance of NPH (at 380 nm) vs. concentration of $CN^-$ plot for determination of limit of detection (LOD) in aqueous medium.

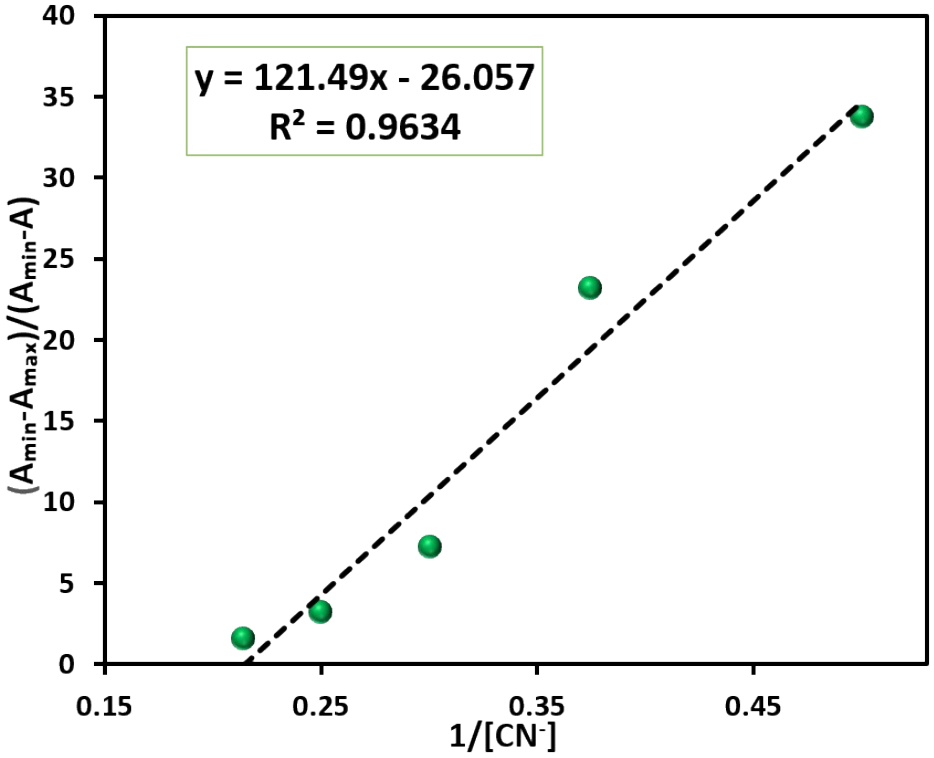


**Fig. S14** Benesi–Hildebrand plot of UV for determination binding constant of NPH and $CN^-$.

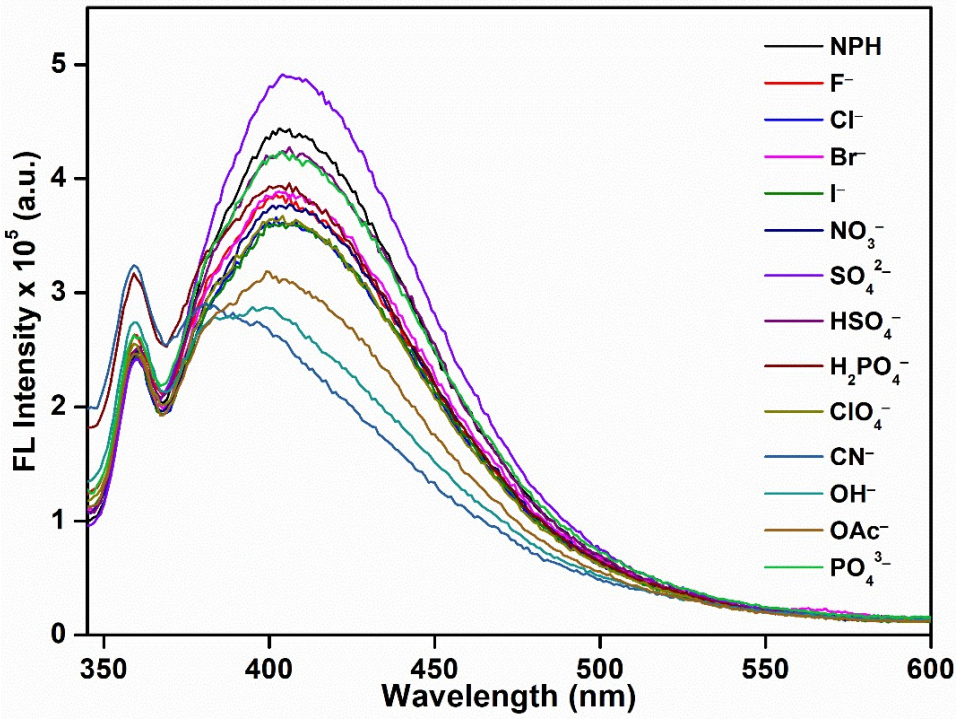


**Fig. S15** Fluorescence spectrum of NPN with various anions.

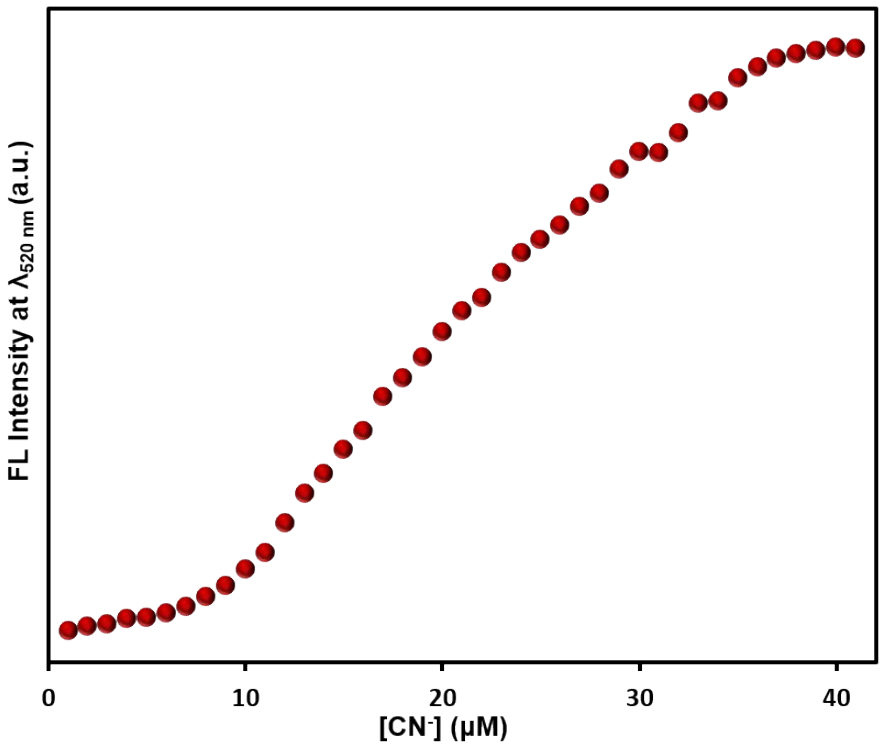


**Fig. S16** Fluorescence intensity of NPH with incremental addition of $CN^-$ (0-27 μM) at 520 nm.

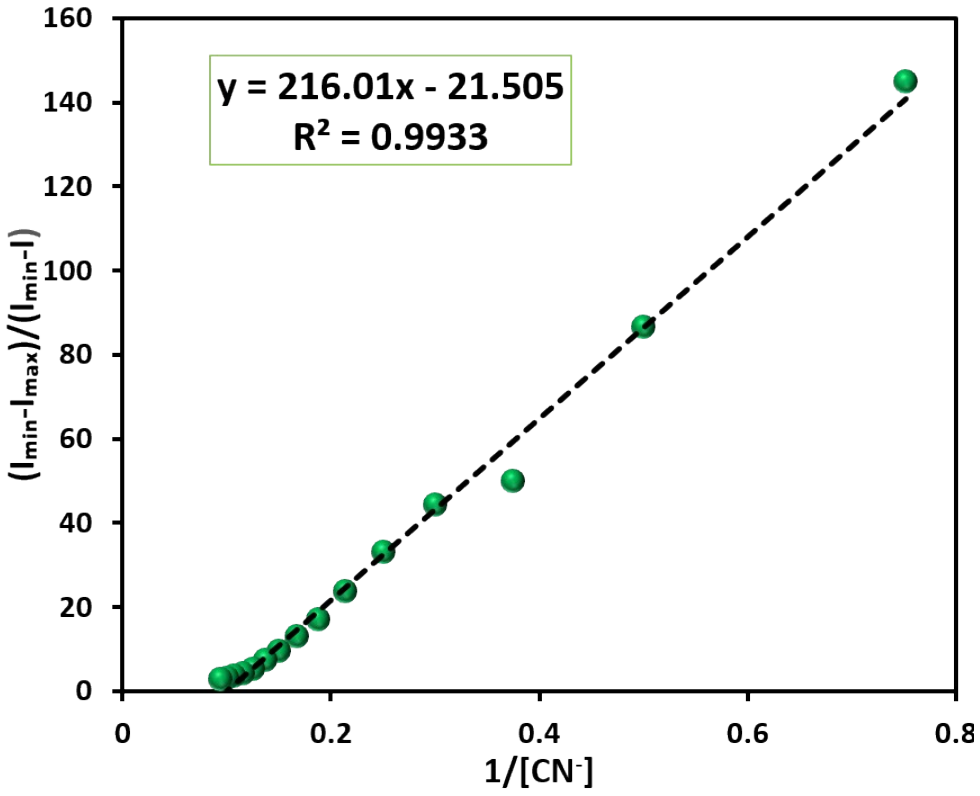


**Fig. S17** Benesi–Hildebrand plot of Fluorescence for determination binding constant of NPH and $CN^-$.

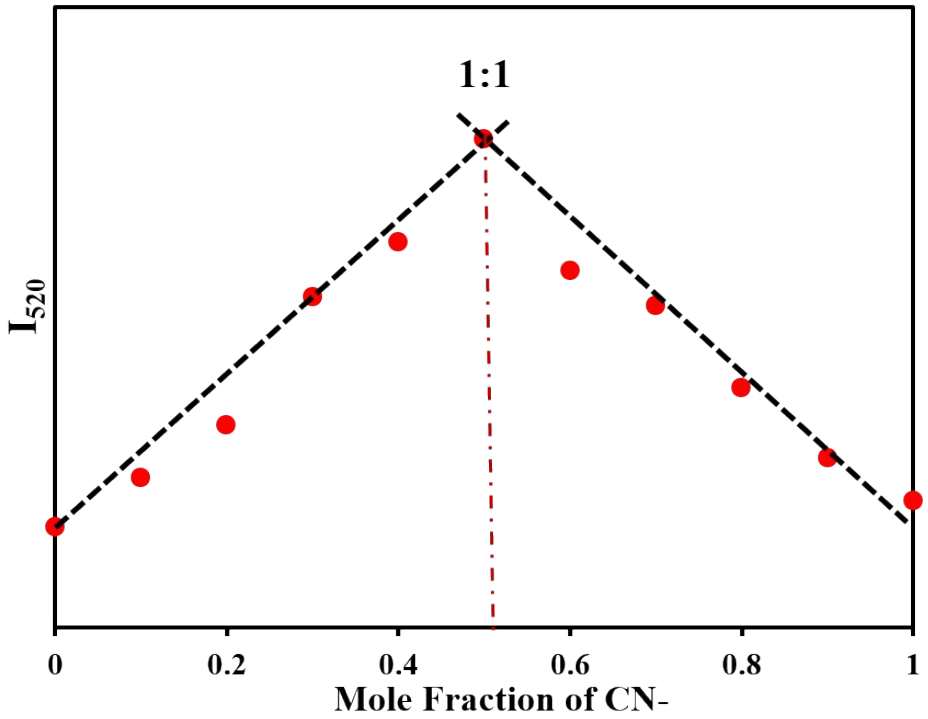


**Fig. S18** Job's plot for NPH + $CN^-$ from fluorescence emission spectrum.

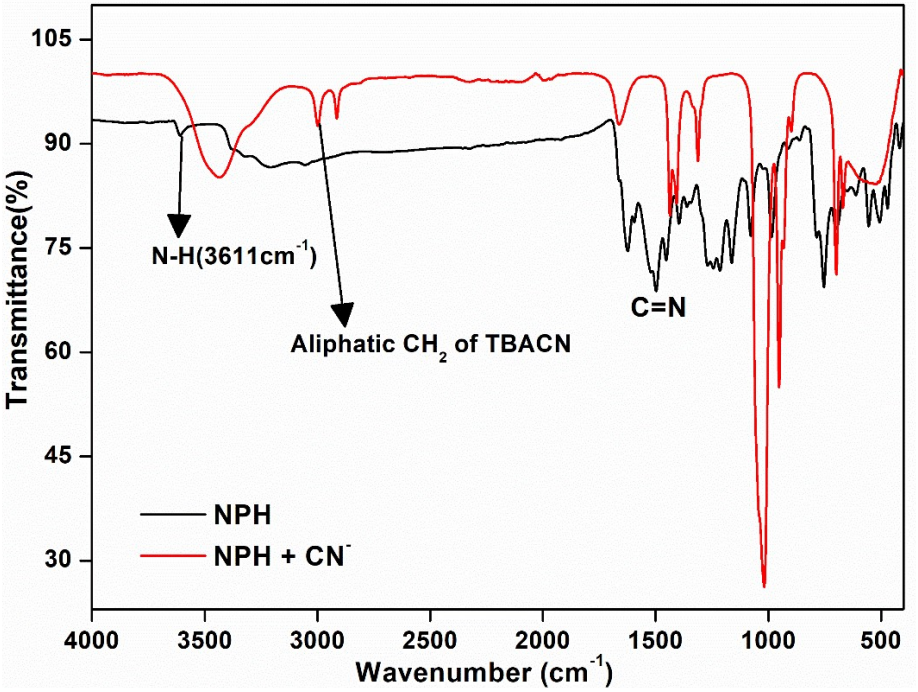


**Fig. S19** Merged FTIR spectra of NPH and NPH-TBACN.

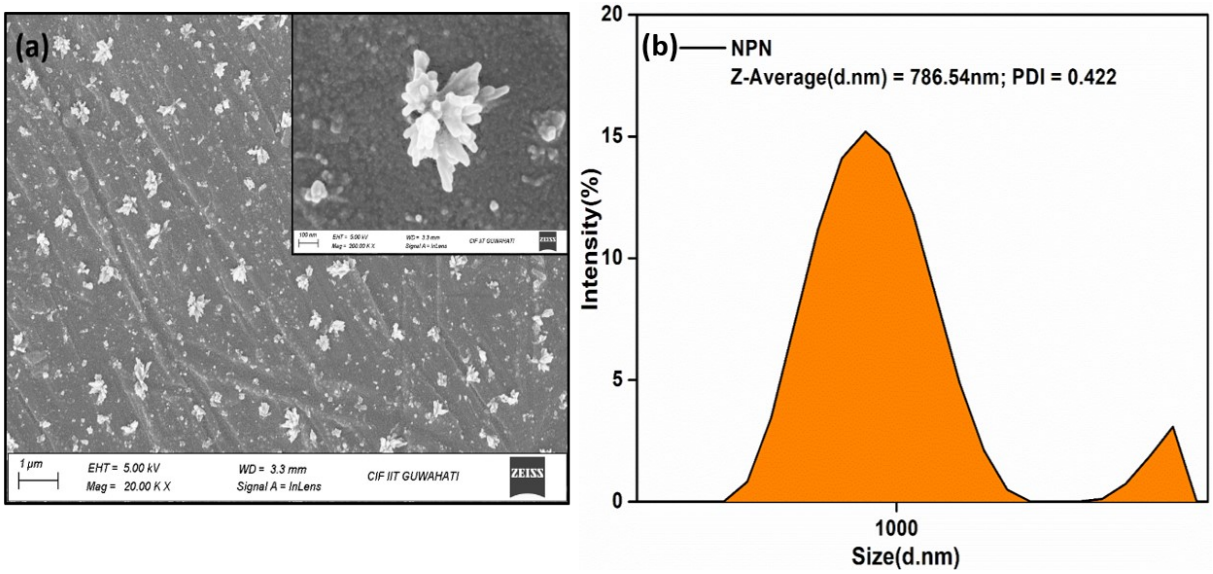


**Fig. S20** (a) FESEM image of NPN, and (b) DLS-based particle size analysis of NPN.

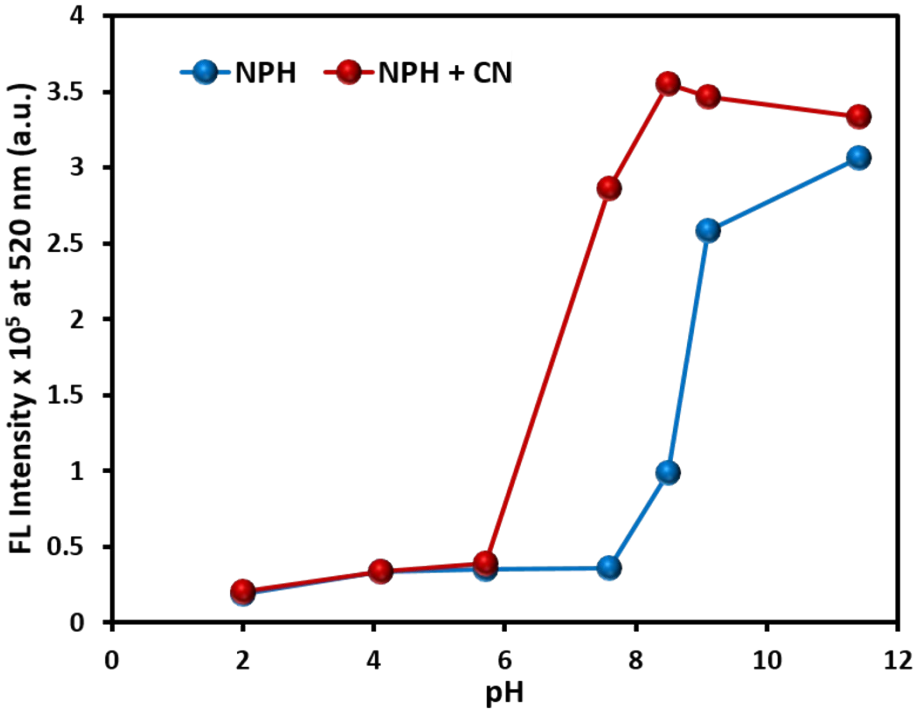


**Fig. S21** Fluorescence emission spectra of NPH and NPH + $CN^-$ at 520 nm in different pH (2-11).

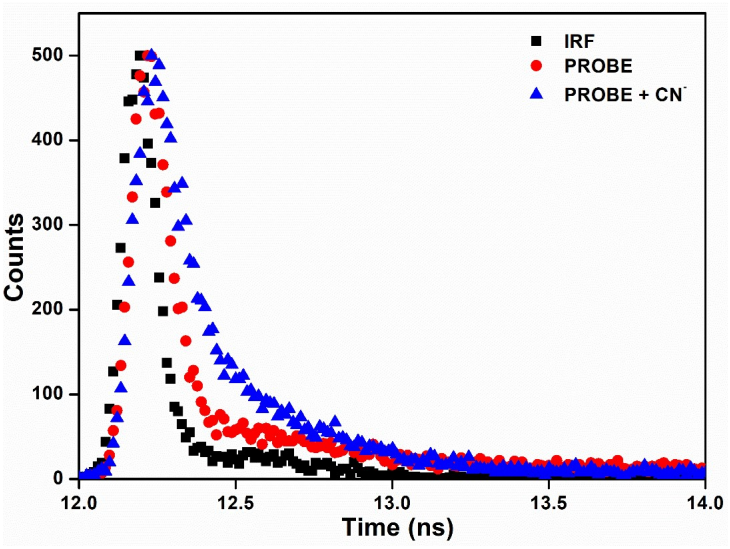


**Fig. S22** Time-resolved photoluminescence spectra of NPH and NPH+$CN^-$ in aqueous medium at 25 °C.

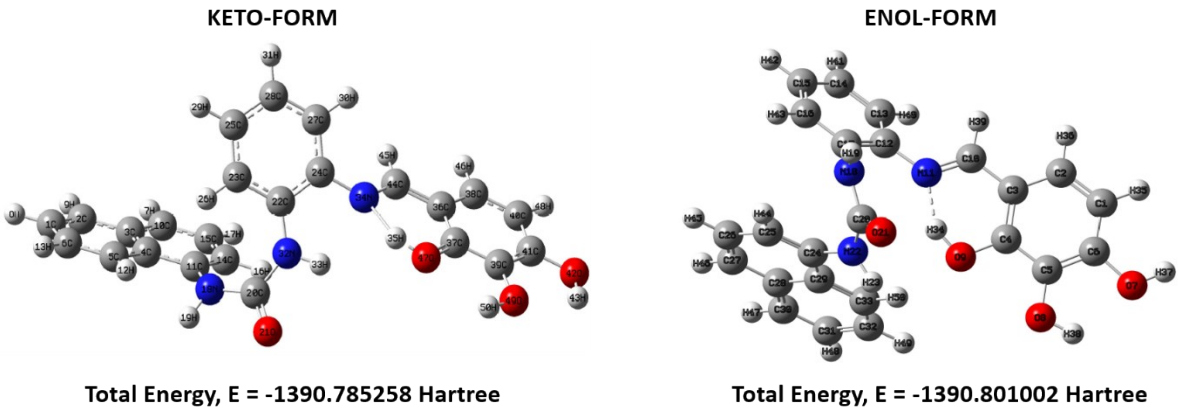


**Fig. S23** Optimized structures of the NPH tautomers at the B3LYP/6-31G level.

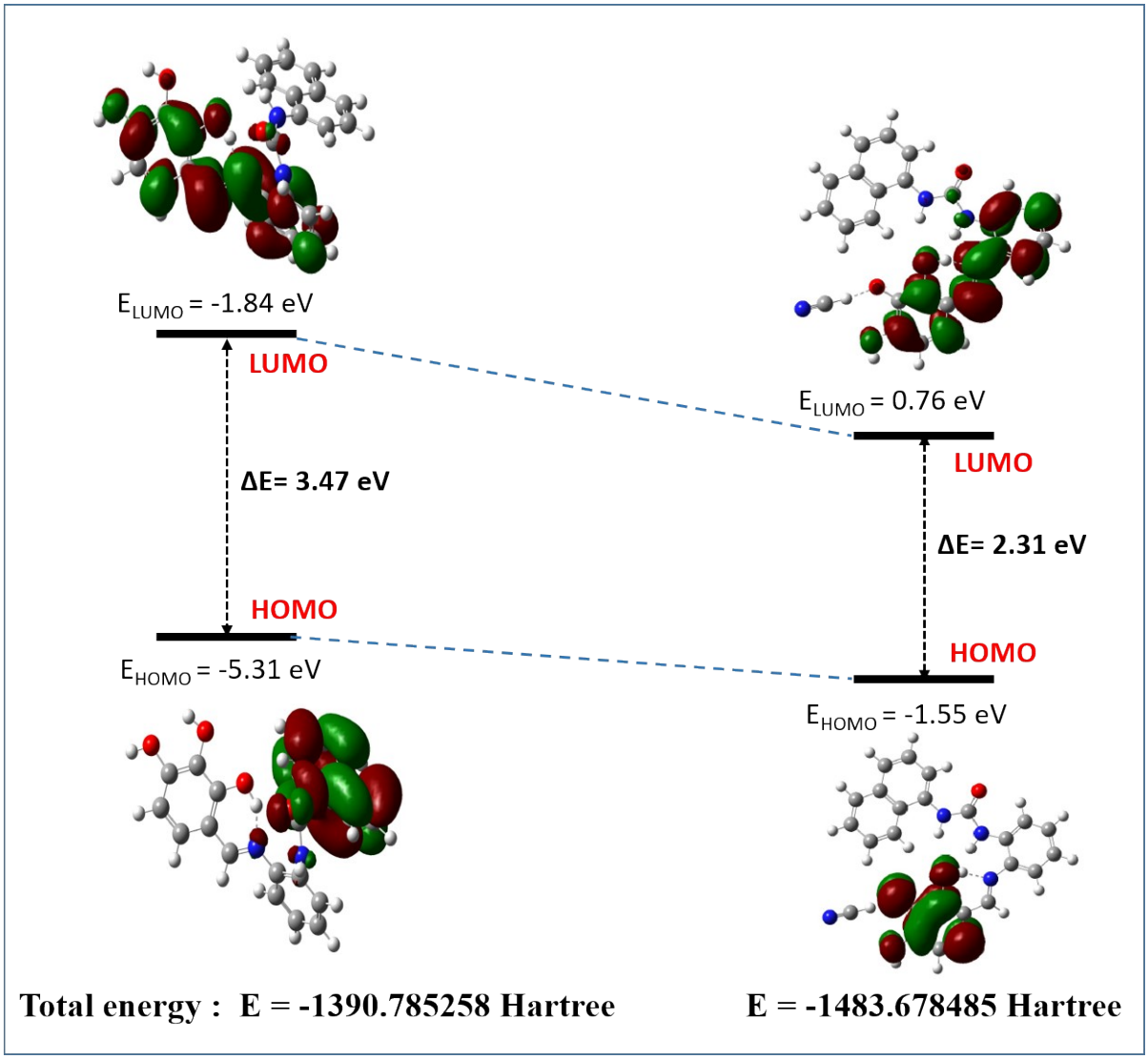


**Fig. S24** The HOMO-LUMO diagram of NPH and NPH-$CN^-$ calculated at the B3LYP/631G level.

**Table S1.** A comparison table of some reported cyanide chemo-sensors.

| Sl. No. | Receptor | Solvent System | Limit of Detection (LOD) | References |
|---|---|---|---|---|
| 1. | Present Work (Urea-based polyphenol Receptor) | Aqueous solvent | 1.36 μM | |
| 2. | Azobenzene-based chemosensor | $CH_3CN$ | 1.1 μM | [1] |
| 3. | Quinoxaline-based Schiff base chemosensor | $CH_3CN$ | 21 μM | [2] |
| 4. | Zinc coordination polymer-based chemosensor bearing ditert-butyl-bipyridine | buffered aqueous solutions (pH=7) | 0.90 μM | [3] |
| 5. | Benzildihydrazone-based sensor | $CH_3OH$-$H_2O$ (2/1, v/v) | $1.5 \times 10^{-7}$ M | [4] |
| 6 | Benzo-Hemicyanine-Based Probe | 1:1 DMSO/$H_2O$ (v/v) | 0.43 μM | [5] |
| 7 | Copper metallogel-based chemosensor | Aqueous solvent | 1.09 μM | [6] |
| 8 | Coumarin functionalized chemosensor | $CH_3CN$ | $5.79 \times 10^{-8}$ M. | [7] |
| 9 | Hydrazide based Cr(III) chemosensor | DMSO–H2O (9:1, v/v) and THF. | 3.26 mM | [8] |
| 10 | Nitrobenzoxadiazole (NBD)-antipyrine conjugate receptors | Aqueous methanol medium (1 : 1, v/v). | $1.67 \times 10^{-7}$ M | [9] |

**Table S2.** Quantum Yield calculations.

| **Sample** | **Integrated Emission** | **Abs at 380 nm** | **Refractive Index** | **Quantum Yield (φ) (%)** |
|---|---|---|---|---|
| **Quinine Sulphate** | $1.36 \times 10^9$ | 0.018903 | 1.33 | **54 (Known)** |
| **NPH** | $1.88 \times 10^6$ | 0.07414 | 1.33 | 0.02 |
| **NPH + $CN^-$** | $2.57 \times 10^7$ | 0.232 | 1.33 | 0.08 |

**Table S3.** DPPH radical scavenging activity (%) of the synthesized compounds (NPH and NPN) at different concentrations (μM).

| SL No. | CONCENTRATION (μM) | PERCENTAGE OF INHIBITION (%) NPH | PERCENTAGE OF INHIBITION (%) NPN |
|---|---|---|---|
| **1** | 10 | 36.43 | 15.78 |
| **2** | 20 | 53.06 | 17.63 |
| **3** | 30 | 68.71 | 18.36 |
| **4** | 40 | 86.23 | 23.69 |
| **5** | 50 | 97.02 | 24.43 |

**Table S4.** Fluorescence decay parameters.

| Sample | $\tau^1$ | $\tau^2$ | $\alpha^1$ | $\alpha^2$ | $\chi^2$ |
|---|---|---|---|---|---|
| **NPH** | 70.662 | 29.338 | 0.218 | 4.157 | 1.015 |
| **NPH + $CN^-$** | 39.505 | 60.495 | 0.101 | 3.852 | 1.001 |

**Table S5.** Optimized structure of NPH-$CN^-$ with other possible locations of complexation in NPH molucule.

| HOMO | LUMO | Total Electronic Energy |
|---|---|---|
| 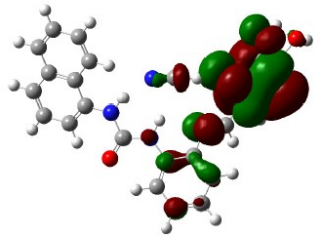 $E_{HOMO}$ = -0.07024 Hartree (-1.91 eV) | 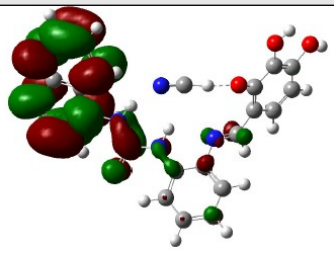 $E_{LUMO}$ = 0.05186 Hartree (1.41 eV) | E = -1483.673987 Hartree |
| 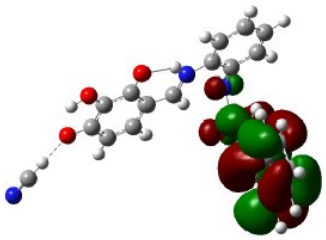 $E_{HOMO}$ = -0.21389 Hartree (-5.82 eV) | 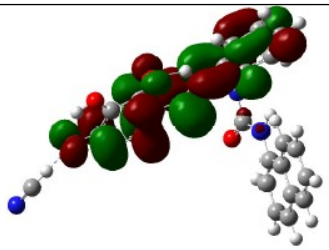 $E_{LUMO}$ = -0.10141 Hartree (-2.76 eV) | E = -1483.582362 Hartree |
| 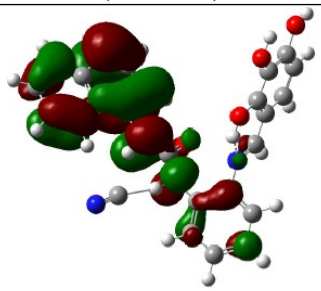 $E_{HOMO}$ = -0.08907 Hartree (-2.42 eV) | 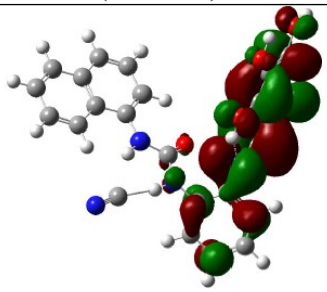 $E_{LUMO}$ = 0.03121 Hartree (-0.85 eV) | E = -1483.657542 Hartree |
| 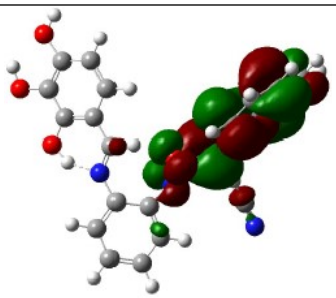 $E_{HOMO}$ = -0.06863 Hartree (-1.87 eV) | 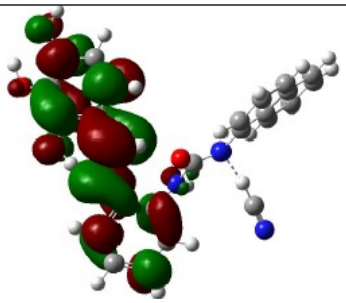 $E_{LUMO}$ = 0.03458 Hartree (-0.94 eV) | E = -1483.654136 Hartree |

| Sample | Spiked amount (µM) | Detected Amount (µM) | Percentage Recovery (%) |
|---|---|---|---|
| River Water | 5 | 4.53 | 90.62 |
| Drinking Water | | 4.61 | 92.31 |
| Tap Water | | 4.308 | 86.16 |

**Table S6.** Determination of cyanide ($CN^-$) concentration in water samples.

## REFERENCES:


[1] X. Cheng, Y. Zhou, J. Qin and Z. Li, 2012, *ACS Appl. Mat. Interfaces*, **4**, 2133-2138.

[2] H. Ghafoor, A. Hussain, S. Hussain, Z. Shafiq, K. Mahmood, N. Ahmed, M. Yar, K. Ayub, X. Hao, Z. Changjin and A. Ali, 2024, *J. Mol. Struct.*, **1308**, 138082.

[3] L.D. Rosales-Vázquez, J. Valdes-García, I.J. Bazany-Rodríguez, J.M. German-Acacio, D. Martinez-Otero, A.R. Vilchis-Nestor, R. Morales-Luckie, V. Sanchez-Mendieta and A. Dorazco-Gonzalez, 2019, *Dalton Trans.*, **48**, 12407-12420.

[4] R. Chandra, A. Ghorai and G.K. Patra, 2018, *Sens. Actuators B Chem.*, **255**, 701-711.

[5] K. Magesh, N. Vijay, S.P. Wu and S. Velmathi, 2023, *J. Agric. Food Chem.*, **71**, 1190-1200.

[6] A. Sebastian and E. Prasad, 2020, *Langmuir*, **36**, 10537-10547.

[7] T. Devendhiran, K. Kumarasamy, M.C. Lin and Y.X. Yang, 2021, *Inorg. Chem. Commun.*, **134**, 108951.

[8] O.R. Shehab and A.M. Mansour, 2023, *J. Mol. Struct.*, **1281**, 135082.

[9] T. Anand and M. Sankar, 2020, *Anal. Methods*, **12**, 4526-4533.